

Photocatalytic Reduction of Chromium (VI) in a Typical Hides and Skin Industrial Wastewater using ZnO/ γ -Al₂O₃ Photocatalyst under Visible LIGHT

Israel Ogbonnaya¹ and Prof. F. Aberuagba²

^{1,2} Department of Chemical Engineering,
School of Infrastructure, Process Engineering and Technology,
Federal University of Technology,

Minna, Niger State,

¹ Scientific Equipment Development Institute,

Minna, Niger State,

Nigeria.

ABSTRACT

Photocatalysis is an advanced oxidation process that can degrade and mineralize organic pollutants in wastewater to carbon dioxide and water which was employed in this study. Tannery effluent was treated via batch photoreduction using Zinc oxide photocatalyst supported on γ -Al₂O₃ and irradiated under visible light at the ambient condition of temperature. Zinc oxide obtained from Zinc ore and γ -Al₂O₃ prepared from local kaolin were used to synthesize the ZnO/ γ -Al₂O₃. The synthesized photocatalyst was characterized by Brunnaer Emmett Teller (BET), X-ray Diffraction Spectroscopy (XRD), Scanning Electron Microscope (SEM), and X-ray Fluorescence (XRF). The result of the analysis reveals that the total surface area, total pore volume and mean pore size of the photocatalyst prepared were 65.452 m²g⁻¹, 0.151 cm³g⁻¹ and 9.892 nm respectively. The photocatalyst is crystalline and the SEM image shows the presence of pores. The ZnO/ γ -Al₂O₃ was used as a photocatalyst to reduce Chromium (VI) of a typical tannery wastewater. 96% reduction of 20 mg/L of Cr (VI) was achieved at 60 min, pH of 3, and a photocatalyst dosage of 2.5 g/L under visible light of 400 W intensity. The kinetic study revealed that the photoreduction was fitted into the pseudo-first-order Lagmuir-Hinshelwood kinetic model. This research demonstrated that ZnO/ γ -Al₂O₃ photocatalyst was effective in the photoreduction of the selected response for the treatment of tannery wastewater.

Key Words: Photocatalysis, ZnO, ZnO/ γ -Al₂O₃, Tannery wastewater.

1. INTRODUCTION

Since ancient times, processing of hides and skin by tanning as a means of conversion to leather has been an important activity. Several processing stages of the raw hides involves treatment with variety of chemicals to obtain the end product and a tannery wastewater having a mixture of biogenic materials of hides and large varieties of organic and inorganic chemicals [1]. According to literature reports, tanneries are associated with water and land pollution, which pose a threat to human, animal and crop life [2]. The composition and constituents of tannery effluent are different from tannery to tannery depending on the size of the tannery, chemicals used for specific processes, amount of water used and type of end product produced by a tannery effluent from a typical tannery. Tanneries generate wastewater in the range of 30-35 LKg⁻¹ with variable pH and large amounts of biological oxygen demand (BOD), chemical oxygen

demand (COD), sodium sulphide, suspended solid, toxic metallic compounds and tannins including Hexavalent Chromium [3-6].

Due to the recalcitrant nature of most of these chemicals, biodegradation is hindered [6]. [7] reported that tannery effluent treatment poses difficulty in achieving the desired effluent discharge standards. Conventional effluent treatment methods involve biological treatment [5] and physio-chemical processes such as coagulation/flocculation, sedimentation [1], ozonation, reverse osmosis, adsorption, ion exchange, and electrolysis [6]. [8] reported that post-biologically treated wastewater still contains non-degradable organic compounds designated bio-recalcitrant organic compounds (BROC). These contaminants are treated using physico-chemical techniques which generate huge amounts of sludge. To mitigate against this problem, focus has been shifted to developing new technologies for effluent treatment and enhancement of the mineralization process of most of the organic contaminant present in the effluent. Photocatalysis, which is advanced oxidation technology is a promising technology for total organic pollutant mineralization [9].

Photocatalysis is the acceleration of a photoreaction in the presence of a catalyst (Photocatalyst) which is activated by adsorbing a photon and is capable of accelerating a reaction without being consumed [10]. Utilization of advanced oxidation technology is a promising method suitable for oxidizing a wide range of bio-recalcitrant waste effluents due to properties such as total degradation/mineralization of pollutants, the formation of congenial products, photocatalytic degradation of organic pollutants, photocatalytic dissolution of water, solar energy conversion and water disinfection [10-11]. In photogenerated catalysis a photochemical reaction is activated on the surface of metal oxide semiconductor with simultaneous oxidation-reduction reactions taking place. The first reaction takes place as a result of photo-induced positive holes and the second reaction is as a result of photo-induced negative electrons [12], followed by the generation of reactive radicals ($O_2^{\circ-}$, OH° , HOO°) that attack the aryl ring of the organic pollutants which leads to the degradation and mineralization to CO_2 and H_2O [11]. Considerable research work has been carried out on quite a number of photocatalysts such as Titanium dioxide (TiO_2), Zinc oxide (ZnO), Iron (II) oxide (Fe_2O_3), Zirconia (ZrO_2), Vanadium (v) oxide (V_2O_5), Niobium pentoxide (Nb_2O_5) and tungsten trioxide (WO_3) and have been extensively used for control of pollutant in wastewater [13-15]. [16] reported that considering the known and researched photocatalyst there is a wider application of ZnO due to factors such as availability, stability, low cost, and favourable band gap energy.

Zinc oxide (ZnO), an important inorganic material with its excellent physical and chemical properties which includes high chemical stability, high electrochemical coupling coefficient, broad range radiation absorption and high photostability, is a multifunctional material [17-18]. And is dominating the photocatalysis field as an efficient substitute for successful green environmental management system due to its outstanding attributes such as direct and wide band gap of about 3.37eV in the near UV spectra region with wave lengths below 387nm, strong oxidation ability, good photocatalytic property, and a large free-exciton binding energy [19]. Supported ZnO nanostructure is a promising candidate because of its structure, porosity and properties. It has the potential to improve the efficiency of catalytic reaction and with its immobilization characteristic for a one step easy removal of the catalyst from the reaction mixture, enabling the nano-sized catalysts to be cleaned, reused, and to yield catalyst free products [10].

A number of transition metals such as Co, Ag, Mn, Pd, Bi, Sm, Ce, Al, were used as dopants for ZnO to improve its photocatalytic activity. Among these support for ZnO photocatalyst, Al-supported ZnO has received considerable attention because of its unique physicochemical properties as well as the merit of cheap raw materials [20]. [21] Stated in his work that the doping of Alumina in ZnO increases the specific surface area which results in a better activity in the photocatalytic decomposition of methylene blue under UV irradiation. Recently [22] also reported that, in the photocatalytic degradation of methyl orange under visible light irradiation, the Zinc oxide photocatalyst supported on 4% of γ -Alumina exhibits higher activity compared to unsupported ZnO and they attributed the enhanced activity to extended light absorption, inhibition of electron-hole pair's recombination and increasing adsorptivity of reactant molecules on the surface of catalyst powders.

In this research work, optimum response obtained from Response Surface Methodology will be used to prepare Zinc oxide photocatalyst supported on γ - Al_2O_3 for the photoreduction of Chromium (VI), biological oxygen demand (BOD), chemical oxygen demand (COD) and pH of a typical hides and skin industry wastewater. The effect of

operating conditions such as photocatalyst dosage, irradiation time, initial pH, initial concentration and light intensity will be investigated. The photoreduction kinetics will be studied from the data obtained from the photoreduction of the tannery effluent.

2. MATERIALS AND METHODOLOGY

All the chemicals used for the experiment was purchased from Pamlac Chemicals, Minna, Niger State and are of analytic grade. Local Kaolin and Zinc ore was obtained from Kutigi, Niger State and Enyigba lead-zinc mine pit, Abakiliki, Ebonyi State respectively. The tannery wastewater was obtained from the retanning and dyeing steps of Maimuda Industries Ltd, Challawa, Kano State, Nigeria. And immediately stored in ice and transported in ice to Minna, Niger State, Nigeria. On arrival, the sample was preserved in cold at a temperature of 4°C.

2.1 PREPARATION OF ZnO/ γ -Al₂O₃

γ -Al₂O₃ was synthesized from local kaolin using the process described by [23] and Zinc oxide was prepared from Zinc ore using the process described by [24-25]. ZnO/ γ -Al₂O₃ was synthesized by wet impregnation technique as reported by [26-28]. 6.40g of Zinc Oxide (ZnO) was measured and suspended in 50 ml of distilled water in a beaker which was stirred at ambient temperature until a homogenous solution was obtained. Then 9.5 g of γ -Al₂O₃ was added into the suspension, and the suspension was stirred vigorously with a magnetic stirrer for 12 hours to form a slurry. The formed slurry was dried at 80°C in an oven for 12 hours and cooled to ambient temperature. The dried sample was crushed, milled to powder, screened through a 150 μ m sieve and then calcined at 800°C for 8 hours to obtain ZnO/ γ -Al₂O₃.

To obtain maximum result, the experiment was repeated and the effects of mass of γ -Al₂O₃, drying temperature, stirring time and mass ratio on the yield of the photocatalyst were investigated through the use of Response Surface Methodology based on composite design. The operational levels of high (+) and low (-) was used to vary factors for optimization of parameters.

2.2 Characterization

X-ray Fluorescence (XRF) analysis was to ascertain the physicochemical composition of the photocatalyst. The morphology of composite particles was observed by SEM Philips XL 30 microscope (PHILIPS). The samples were coated with an Au/pd film and the SEM images were obtained by using a secondary electron detector. The BET was used to measure the surface area and porosity of the sample, BET TRISTAR 3000 analyser was used. Before the analysis approximately 0.2 g of the sample was weighed and degassed under N₂ for 4 hours ambient temperature at 150°C to remove moisture. The degassed sample was later analysed for physisorption of adsorbate (nitrogen) by the adsorbent in the liquid nitrogen on the surface.

2.3 Determination of Chromium (Vi) Concentration

The concentration of Chromium (Cr) in the effluent sample was determined by Atomic Absorption Spectrophotometric method on 470 nm by using a UV spectrometer (Shimadzu UV-240 spectrophotometer) [4].

3. PHOTOCATALYTIC PROCESS

3.1 Effect of irradiation time

100 ml of the effluent was collected and placed in a beaker, followed by the addition of 0.1 g of the photocatalyst. It was magnetically stirred for 60 min in the dark. Samples were collected after 60 min of reaction and analysed for Chromium (VI), BOD and COD concentrations. Immediately after adsorption in the dark stage for 1 hr, the mixture of effluent and the photocatalyst in the beaker was exposed to visible light irradiation by a 400 W halogen lamp under stirring. Samples were taken after 0, 5, 10, 20, 40 and 60 min from the start of irradiation and analysed for Chromium (VI), BOD and COD concentrations.

3.2 Effect of photocatalyst dosage

To determine the effect of photocatalyst dosage, 100 ml of the effluent was measured and placed in a beaker, 0.5 g of the photocatalyst was then measured and added to content of the beaker, the beaker was then placed on a magnetic stirrer. The content of the beaker was continuously stirred in the dark for 60 min after which a 5 ml of the sample was taken for analysis. The content of the beaker was then exposed to visible light while it was continuously stirred for another 60 min. After the photocatalytic reaction of the treated water 5 ml sample was then collected for analysis, the same procedure was repeated for varying amounts of photocatalyst for Chromium (VI), BOD and COD concentrations.

3.3 Effect of initial pH of wastewater

100 ml of the effluent was measured and placed in a beaker, sodium hydroxide and hydrochloric acid solution whose concentration is known was added to it to adjust the pH of the effluent. For any addition of sodium hydroxide and hydrochloric acid solution, a pH meter was used to determine the pH of the effluent, 5 mL of effluent was then taken for analysis, the effluent was then magnetically stirred in the dark for 60 min and again 5 ml sample was collected for analysis. The effluent was further exposed to light for another 60 min and again 5 ml sample of the effluent was taken for analysis. The same procedure was repeated for pH 2 to 12 for Cr (VI), BOD and COD concentrations.

3.4 Effect of initial concentration

100ml of effluent was measured and placed in a beaker. Distilled water was used to vary the concentration of Cr (VI), BOD and COD, a 5 ml of effluent was taken for analysis. The effluent was then magnetically stirred in the dark for 60 min and again 5 ml sample was collected for analysis. The effluent was further exposed to visible light for another 60 min and again 5 ml sample of the effluent was taken for analysis. The same procedure was repeated for 20, 40, 60, 80 and 100 mg/L initial concentrations of Cr(VI), COD and BOD.

3.5 Effect of light intensity

To determine the effect of light, 100 ml of the effluent was measured and placed in a beaker, exposed to 100 W tungsten lamp and continuously stirred for 60 min, 5 ml of the sample of the wastewater was then taken for analysis. This procedure was repeated for 200 and 400 W tungsten lamp.

3.6 Kinetics of degradation

Kinetics study was carried out based on the initial concentration of the effluent. The photocatalytic reaction kinetics of organic compounds is often described by the pseudo first order approximation of the Langmuir–Hinshelwood model [29-30]. The equation given as:

$$\ln \left[\frac{C_0}{C} \right] = Kt \quad 3.1$$

Where:

K = Apparent rate constant for the photocatalytic reduction

T = Irradiation time

C₀ = Initial concentration

C = Final concentration

3.6 Determination of percentage degradation

The percentage degradation of the tannery effluent was obtained by the following relationship

$$\% \text{ Degradation} = \frac{C - C_0}{C} \times 100 \quad 3.2$$

Where;

C₀= Initial Concentration of tannery effluent before degradation.

C= Initial Concentration of tannery effluent after degradation.

4. RESULTS AND DISCUSSION

4.1 Characterization of the prepared ZnO/ γ -Al₂O₃ photocatalyst using XRF SEM, and BET analysis

The following results were obtained after the characterization of ZnO/ γ -Al₂O₃ photocatalyst;

4.2 X-ray Fluorescence (XRF) analysis

XRF analysis was used to determine the ZnO content of the ZnO/ γ -Al₂O₃ catalyst. The result as can be seen in Table 1 shows that there are two main compositions of the catalyst being 44.421% of Zinc oxide (ZnO) and 53.303% γ -Al₂O₃. Meanwhile, the remaining 2.276% is impurities, which consist of SO₃ (1.905%), SiO₂ (0.173%), and CaO (0.198%). As expected, Al₂O₃ was the highest component, followed by ZnO and impurities, respectively. This result shows that the prepared catalyst has high purity, approaching 98%.

Table 1. X-Ray Fluorescence (XRF) result of ZnO/ γ -Al₂O₃

COMPOSITIONS	WEIGHT PERCENTAGE
ZnO	53.303
γ -Al ₂ O ₃	44.421
SO ₃	1.905
SiO ₂	0.173
CaO	0.198
Total	100

4.3 Brunauer-Emmet Teller (BET) analysis

The specific surface area of synthesized ZnO/ γ -Al₂O₃ photocatalyst was measured using Brunauer-Emmet Teller (BET) as shown in Table 2. The BET surface area, pore volume and mean pore size were 65.452 m²g⁻¹, 0.151 cm³g⁻¹ and 9.892 nm, respectively. This result is similar to that obtained by [31]. The surface area of the referenced Alumina supported ZnO photocatalyst was 71.561 m²g⁻¹, the pore volume was 0.137 cm³g⁻¹ and the mean pore size was 8.149 nm.

Table 2. Brunauer-Emmet Teller (BET) Result of ZnO/ γ -Al₂O₃

ZnO/ γ -Al ₂ O ₃ PHOTOCATALYST	SURFACE AREA (m ² g ⁻¹)	PORE VOLUME (cm ³ g ⁻¹)	MEAN PORE SIZE (nm)
Synthesized	65.452	0.151	9.892
Anandan et al., (2010)	71.561	0.137	8.149

4.4 Scanning Electron Microscope (SEM) analysis

The morphological and structural characterization of the synthesized ZnO/ γ -Al₂O₃ was investigated using Scanning Electron Microscope (SEM) analysis. The SEM image of the ZnO/ γ -Al₂O₃ photocatalyst is shown in Figure 1. The result indicates that the Zinc Oxide (ZnO) with rod-like shape, which is a typical morphology of Zinc oxide particle, was uniformly distributed on γ -Alumina surface which has a flower-like structure. [32-34] reported similar result.

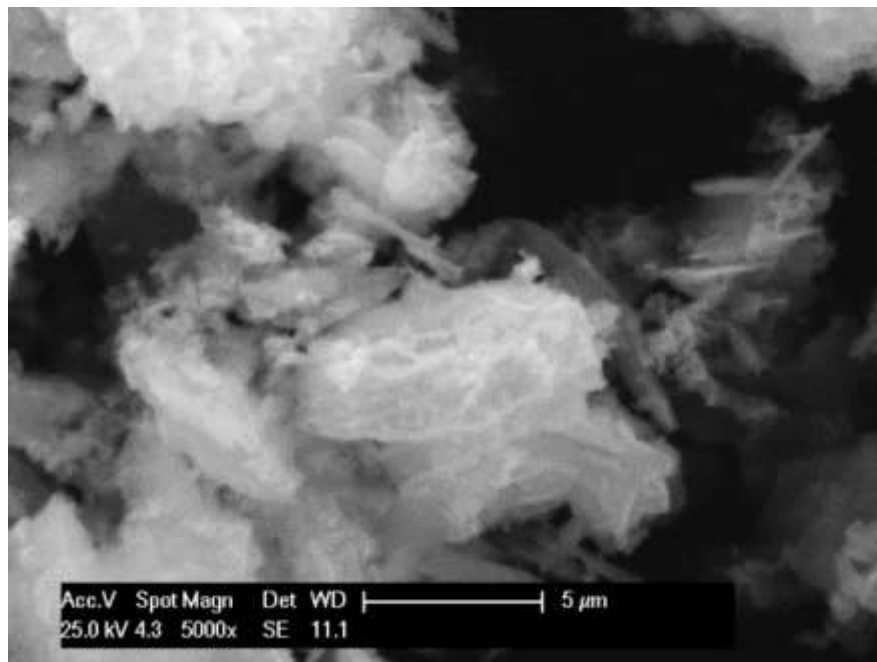


Figure 1. SEM result of ZnO/ γ -Al₂O₃

4.5 Chromium (VI) Reduction

Photodegradation was carried out for Chromium and the effects of photocatalyst dosage, irradiation time, initial pH, Initial concentration, light intensity, and degradation kinetics was studied.

4.6 Efficiencies of pure ZnO/ γ -Al₂O₃, γ -Al₂O₃, pure ZnO, visible light/ZnO, and visible light/ZnO/ γ -Al₂O₃

To evaluate the effect of various processes involved in the photocatalytic reduction of Chromium (VI), the efficiencies of pure ZnO/ γ -Al₂O₃, γ -Alumina, pure ZnO, Visible light/ZnO, and Visible light/ZnO/ γ -Al₂O₃ in the reduction of Chromium (VI) were separately evaluated using the raw wastewater as shown in Figure 2. The efficiencies of pure ZnO was 27.1% and pure γ -Alumina was 33.2% and they were insignificant for the removal of Chromium through the adsorption within the reaction time of 60 min. The higher adsorption capacity of ZnO/ γ -Al₂O₃ composite (61.6%) for the removal of Chromium ions compared to both pure ZnO and pure γ -Al₂O₃ would be favorable for the subsequent enhanced photocatalytic reduction of Chromium over the surface of the ZnO/ γ -Al₂O₃ composite.

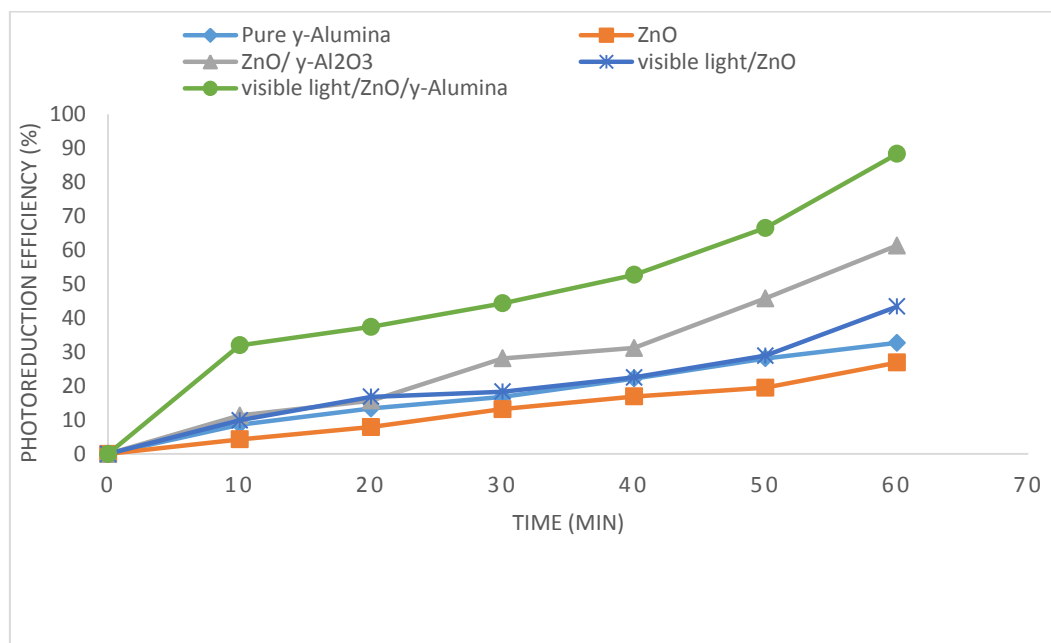


Figure 2. Efficiencies of pure ZnO/ γ -Al₂O₃, γ -Al₂O₃, pure ZnO, Visible light/ZnO, and Visible light/ZnO/ γ -Al₂O₃

As can be seen from Figure 2, the efficiency of the visible light/ ZnO/ γ -Al₂O₃ process for the reduction of Chromium (VI) was about 88%, which was more effective than the visible light/ZnO process which reduced 43.7% of Chromium (VI). The higher efficiency of the ZnO/ γ -Al₂O₃ process compared to the visible light/ZnO process indicating the synergy between ZnO and γ -Al₂O₃.

4.7 Effect of photocatalyst dosage

To investigate the effect of photocatalyst dosage on the photocatalytic reduction of Cr(VI), the dosage was varied from 0.5 to 5.5 g/L, while the initial pH, initial Chromium concentration, and reaction time were constant at 4, 60 mg/L, and 60 min respectively. As can be seen from Figure 3, by increasing photocatalyst dosage from 0.5 to 2.5 g/L the photocatalytic reduction of Chromium was increased from 35.7 to 88.3% at 60 min of irradiation, while further increment in the dosage resulted in no significant increase in the reduction of Cr(VI).

At photocatalyst dosage of 4.5 g/L, the photocatalytic reduction of Cr(VI) was obtained to be 97.1%. This behavior can be explained by the increased active sites on the photocatalyst as well as the generation of free electrons in the conduction band during photocatalysis [35]. As the photocatalyst dosage was increased further to 5.5 g/L the photodegradation decreased to 81.8%, this can be attributed to turbidity in the reaction medium.

Due to no significant increase in the reduction of Chromium with increasing photocatalyst dosage from 2.5 to 4.5 g/L, the following experiments were carried out with photocatalyst dosage of 2.5 g/L to evaluate the effect of various processes involved in the photocatalytic reduction of Chromium (VI).

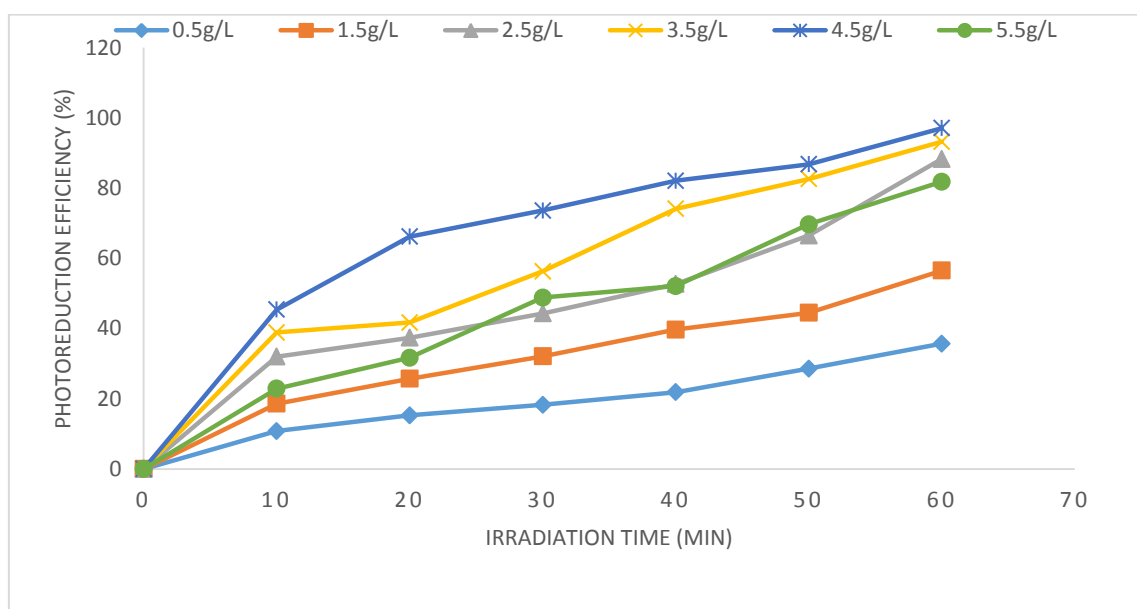


Figure 3. Effect of photocatalyst dosage on the photocatalytic reduction of chromium (VI)

4.8 Effect of irradiation time

The photocatalytic reduction of chromium (VI) was carried out and the effect of irradiation time on Photocatalyst dosage was studied. The experiment was carried out with constant stirring at room temperature for different time intervals from 10 to 60 min. The photoreduction of chromium was 88.3%, 52.7% 44.3% and 32.0% at time intervals of 60, 40, 30, 10 minutes respectively as can be seen in Figure 3. Increase in irradiation time, increased the efficiency of the photocatalyst due to sufficient resident time needed to reduce the hexavalent chromium.

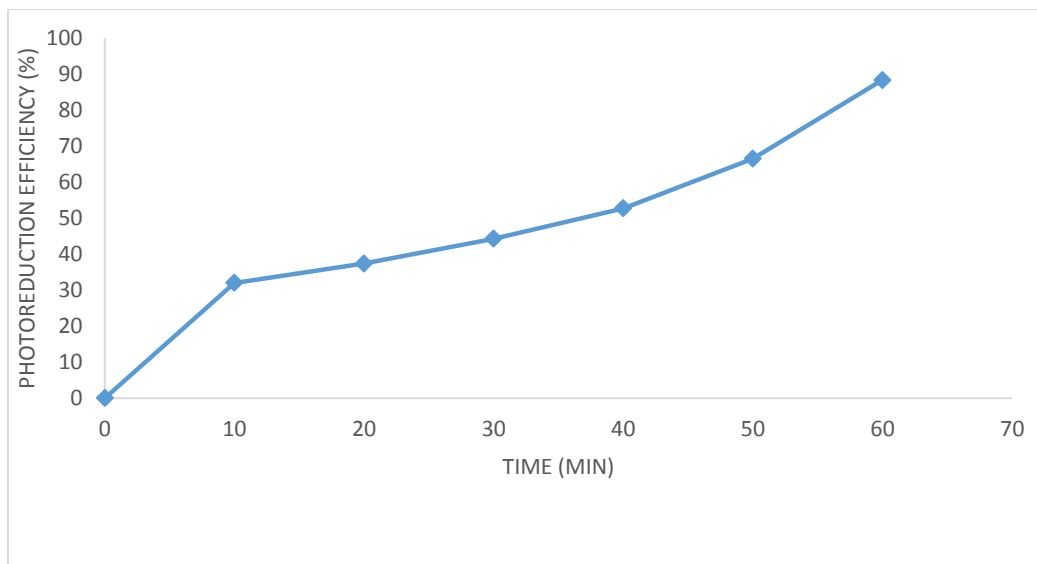


Figure 3. Effect of irradiation time on photocatalytic reduction of chromium

4.9 Effect of initial pH

The effect of initial pH on the photoreduction of Chromium (VI) using ZnO/y-Al₂O₃ photocatalyst was investigated by varying the initial pH from 2 to 11 at a constant photocatalyst dosage of 2.5 g/L at 60 min irradiation time and initial concentration of 60 mg/L. The effect of chromium removal is highly dependent on the pH of the wastewater [36]. As shown in Figure 4, within a reaction time of 60 min, the photoreduction of Cr(VI) was increased from 18.8 to 88.3% with increasing initial pH from 2 to 4 and then decreased to 14.2% when the initial pH concentration reached 11. As shown in figure 4.13, the photocatalytic reduction of Cr(VI) through the ZnO/y-Al₂O₃ photodegradation process at strong acidic and basic pH was much lower than that as pH 4. It is as a result of increase dissolution of ZnO as photocatalyst in strong acidic and basic condition [37-38].

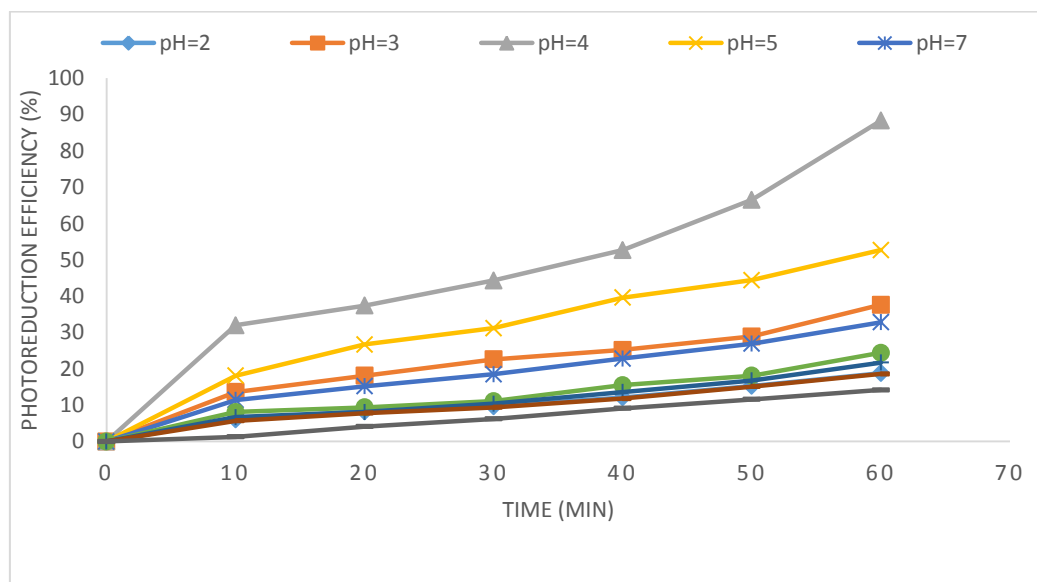


Figure 4. Effect of initial pH on the photocatalytic reduction of Chromium (VI)

4.10 Effect of initial Chromium (VI) concentration

The effect of initial Chromium (VI) concentration on the photocatalytic reduction was evaluated by varying the initial Chromium concentration from 20 to 100 mg/L at constant initial pH of 4, and photocatalyst dosage of 2.5 g/L within reaction time of 60 min as shown in Figure 5. As illustrated, the photocatalytic reduction of Chromium (VI) was increased from 60.7 to nearly 100% with decreasing the initial Chromium concentration from 100 to 20 mg/L at the reaction time of 60 min.

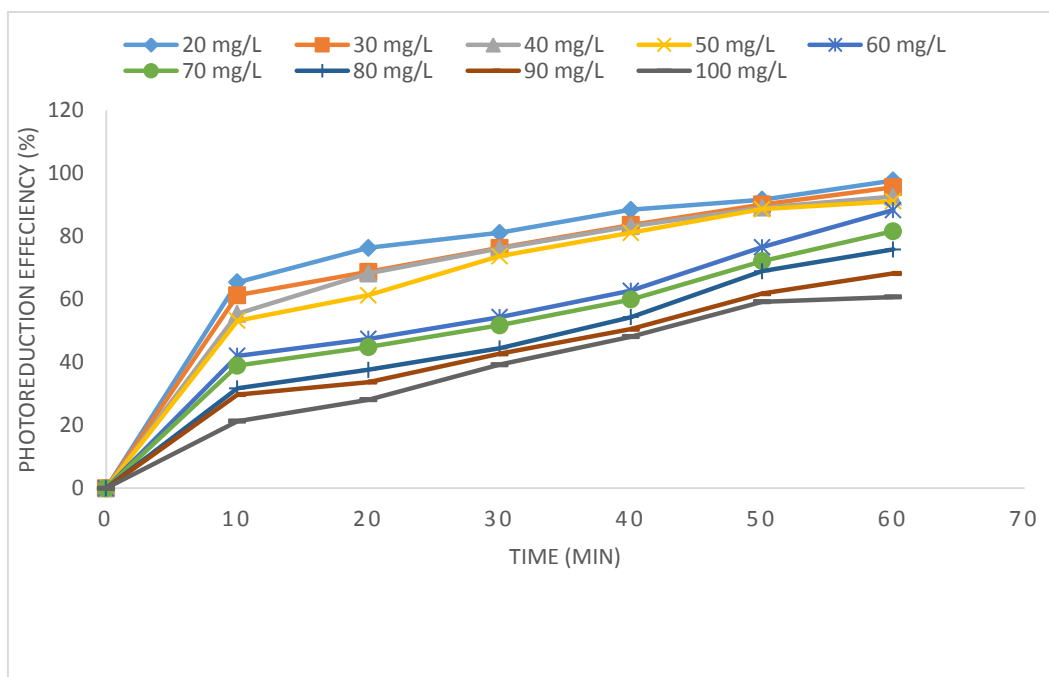


Figure 5. Effect of initial chromium (VI) concentration on photoreduction efficiency

Increasing the initial Chromium concentration results in more Chromium ions adsorbed onto the ZnO/ γ -Al₂O₃ surface, which caused an inhibitive effect on further photocatalytic reduction of Chromium due to inability of the photons to have access to the active sites of the photocatalyst. This lead to insufficient generation of reactive species that is responsible for the reduction of Cr(VI). Similar observation was reported by [39].

4.11 Effect of light intensity

The influence of visible light intensity on the photoactivity of ZnO impregnated on γ -Al₂O₃ in the photoreduction of chromium (VI) is shown in Figure 6. Results shows that reduction percentage increases with increasing light intensity. With an increase in the light intensity, ZnO/ γ -Al₂O₃ absorbs more photons and, therefore, increases the generation rate of photoactive species (electron-hole pairs) on the semiconductor surface, which increased the rate of Chromium photocatalytic reduction. Increase in photoreduction rate of Chromium with enhancement in the light intensity indicates that all the photons were effectively used and the produced electron-hole pairs were consumed more rapidly by chemical reactions than by recombination.

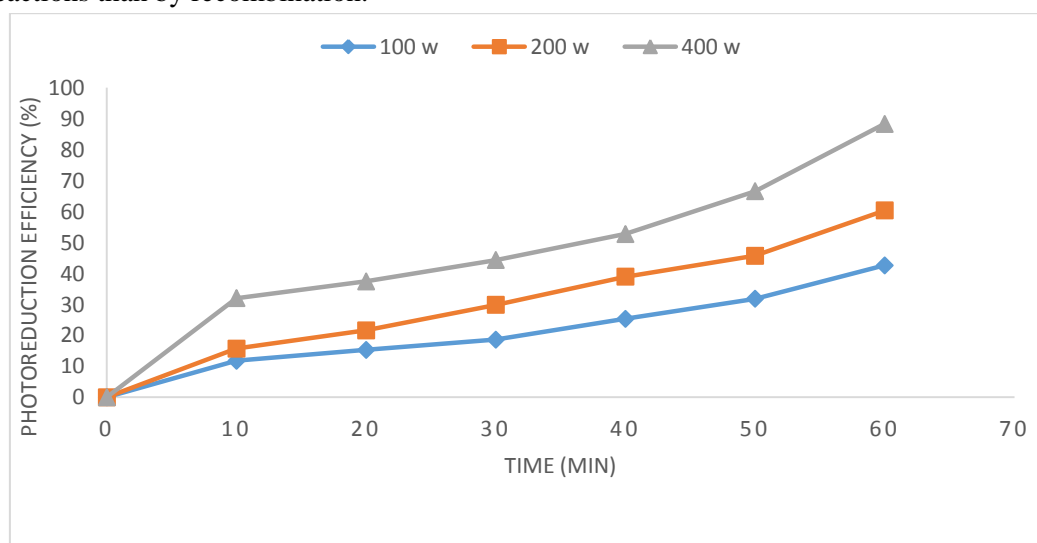


Figure 6. Effect of light intensity on photoreduction efficiency

4.12 Kinetics of Degradation

The kinetics of Chromium degradation was estimated. The kinetics models of the pseudo-first-order model were tested to determine the kinetics rate in the degradation process of Chromium onto the ZnO/y-Al₂O₃ photocatalyst at different irradiation times and Chromium concentrations respectively. The linear fit between $\ln(C_0/C)$ and reaction time t of different initial concentration follows a pseudo-first-order kinetics behavior. The highest correlation coefficients (R^2) was 0.9766 with the least being 0.8739 as shown in Table 3, which indicates that the photoreduction of Cr(VI) fits well with the kinetic model. The rate constants of different initial concentrations of 20, 40, 60, 80, and 100 are 0.0147, 0.487, 0.0293, 0.0543 and 0.0591 min^{-1} respectively.

Table 3. First-order kinetic constants and relative coefficients for photocatalytic reduction of Chromium (VI)

INITIAL (mg/L)	CONCENTRATION	K (min^{-1})	R^2
20		0.0147	0.9228
40		0.487	0.9848
60		0.0293	0.8739
80		0.0543	0.9417
100		0.0591	0.9766

5. CONCLUSION

In this study, photocatalytic degradation of contaminants in tannery wastewater was carried out using ZnO/y-Al₂O₃ in the presence of visible light. The physicochemical analysis of the wastewater was carried out to ascertain the level of Chromium (VI). The total surface area, total pore volume and mean pore size of the photocatalyst prepared were 65.452 m^2g^{-1} , 0.151 cm^3g^{-1} and 9.892 nm respectively. The experimental result shows that at optimum conditions, photocatalyst dosage was determined to be 4.5 g/L for Cr (VI). Maximum photoreduction was observed at pH 4, under 400 W visible light irradiation. It was established that photocatalyst dosage, irradiation time, initial concentration, initial pH and light intensity influences photoreduction efficiency. The photocatalytic reduction fitted the Langmuir-Hinshelwood kinetic model. The calculated values of the correlation coefficient (R^2) value at the optimum conditions is 0.9228.

REFERENCES

- [1] Murugananthan, M., Bhaskar, R. G., Prabhakar, S. (2014). Separation of pollutants from tannery effluents by electro flotation Separation and Purification Technology 40, 69–75.
- [2] Natarajan, T. S., Natarajan, K., Bajaj H. C., Tayade, R. J. (2013). Study on identification of leather industry wastewater constituents and its photocatalytic treatment. *International Journal of Environmental Science and Technology* 10, 855–864 DOI 10.1007/s13762-013-0200-9.
- [3] Rameshraj, D. and Suresh, S. (2011). Treatment of Tannery Wastewater by Various Oxidation and Combined Processes. *International Journal of Environmental Research*, 5(2):349-360, Spring. ISSN: 1735-6865.
- [4] Bhalli, J. A., and Khan, Q. M. (2006). Pollution level analysis in tannery effluents collected from three different cities in Punjab, Pakistan. *Pakistan. Journal of biological sciences* 9(3): 418-421 ISSN 1028-8880
- [5] Durai, C and Rajasimman, M. (2011). Biological treatment of tannery wastewater – A Review. *Journal of environmental science and engineering* (4): 1-17, ISSN 1999-7887, doi:10.3923/jest.2011.1.17.
- [6] Abdel-Aal, E.A., Farghaly, F.E., Abdel-Wahed, R.T., El-Shahat, M.F. (2015). Treatment of Industrial Wastewater Using Advanced Oxidation Processes. *International Journal of Scientific Research in Agricultural Sciences*, 2(Proceedings), 068-078.

- [7] Hasegawa, M. C., Daniel, J. F. de S., Takashima, K., Gisselma A., Batista, da Silva, S. M. C. P. (2014). COD removal and toxicity decrease from tannery wastewater by zinc oxide-assisted photocatalysis: A case study. *Environmental Technology*, DOI: 10.1080/09593330.2013.874499.
- [8] Domenico, C., Puccini, M., Salvadori, M., Seggiani, M., Vitolo, S. (2015). Treatment of Tannery WasteWaters Using Photocatalytic Process with Nanomolecular Materials.
- [9] Natarajan, T. S., Natarajan, K., Bajaj H. C., Tayade, R. J. (2013). Study on identification of leather industry wastewater constituents and its photocatalytic treatment. *International Journal of Environmental Science and Technology* 10, 855–864 DOI 10.1007/s13762-013-0200-9.
- [10] Ali, A. M. (2011). Characterisation of Semi-Conductor Zinc Oxide (ZnO) thin films as Photocatalysts. 1-3
- [11] Raheem, Z., Hameed, A. M. (2015). Photocatalytic Degradation for Methylene Blue Dye Using Magnesium Oxide. *International Journal of basic and applied science*, E-ISSN: 2301-4458; P-ISSN: 2301-8038.
- [12] Fujishima, A., Zhang, X.T., Tryk, D.A. (2008). Titanium dioxide (TiO₂) photocatalysis and related surface phenomena. *Surface Science Reports*, 63, 515-582.
- [13] Carp, H.T., Handraboss, V.L., Natanapatham, L., Karthikeyan, B., Kamalakkannan, J., Prabha, S., Senthilvelan, S. (2015). Effect of bismuth doping on the ZnO nanocomposite material and study of its photocatalytic activity under UV-light. *Material Research Bulletin*, 48 (10), 3707-3712.
- [14] Kudo, A., Miseki, Y. (2009). Heterogeneous photocatalyst materials for water splitting. *Journal of Chemical Society*, 38, 253-278.
- [15] Vinu, R., Madras, G. (2010). Environmental remediation by photocatalysis. *Journal of Indian Institute of Science*, 90, 189-229.
- [16] Muthirulan, P. M., Meenakshisundaram, N. K. (2013). Beneficial role of ZnO photocatalyst supported with porous activated carbon for the mineralization of alizarin cyanin green dye in aqueous solution. *Journal of Advanced Research*, 4, 479–484, doi.org/10.1016/j.jare.2012.08.005.
- [17] Segets, D., Gradl, J., Taylor, R.K., Vassilev, V., Peukert, W. (2009) Analysis of optical absorbance spectra for the determination of ZnO nanoparticle size distribution, solubility, and surface energy. *Journal of American Chemical Society Nanomaterial*, 3, 1703–1710.
- [18] Kołodziejczak-Radzimska, A., Jesionowski T. (2014). Zinc Oxide—From Synthesis to Application: A Review. *Materials*, 7, 2833-2881; doi:10.3390/ma7042833
- [19] Lee, K. M., Lai C. W., Ngai K. S., Juan, J. C. (2016). Recent developments of zinc oxide based photocatalyst in water treatment technology: A review. *Water Research*, 88, 428-448
- [20] Lee H. J., Joo H. K., Seong S. P., Seong S. H., Gun D. L. (2014) Degradation kinetics for photocatalytic reaction of methyl orange over Al-doped ZnO nanoparticles. *Journal of Industrial and Engineering Chemistry. Journal of Chemical Engineering*, 1-16
- [21] Hsiao, K.C., Liao, S.C., and Chen, Y.J. (2007) Material Science Engineering. *Journal of Industrial and Engineering Chemistry*, 447 71–76.
- [22] Ahmad, M., Ahmed, E., Hong, Z.L., Jiao, X.L., Abbas, T., Khalid, N.R. (2013). Enhancement in visible light-responsive photocatalytic activity by embedding Cu-doped ZnO nanoparticles on multi-walled carbon nanotubes. *Applied Surface Science* 285 Part B, 702-712.
- [23] Hosseini, S. A., Niaei, A., Salari, D. (2011). Production of γ -Al₂O₃ from Kaolin. *Open Journal of Physical Chemistry*, 1, 23-27 doi:10.4236/ojpc.2011.12004
- [24] Li, J. Z., Zhong, J.B., Hu, W., Lu, Y., Zeng, J., and Shen, Y.C. (2013). Synthesis of zinc oxide by smelting. *Materials Science in Semiconductor Processing* 16(1), 143-148.
- [25] Cao, L.-Y., Ou, H.-B., and Yao, C.-Y. (2014). Microwave hydrothermal synthesis of K⁺ doped ZnO nanoparticles with enhanced photocatalytic properties under visible-light. *Materials Letters* 118, 17-20.
- [26] Chen, J-C., Tang, C-T. (2007) Preparation and application of granular ZnO/Al₂O₃ catalyst for the removal of hazardous trichloroethylene. *Journal of Hazardous Materials* 142 (2007) 88–96
- [27] Asri, N. P., Soe'eib, S., Poedjojono, B., Suprpto, H. (2017) Alumina supported zinc oxide catalyst for production of biodiesel from kesambi oil and optimization to achieve highest yields of biodiesel. *Journal of Environmental Integration*, 3:3 DOI 10.1007/s41207-017-0043-8

- [28] Alshaibani, M., Yaakob, M., Alsobaai, M., Sahri, M. (2012). Optimization of $\text{pd-b}/\gamma \text{ Al}_2\text{O}_3$ catalyst preparation for palm oil hydrogenation by response surface methodology (RSM). *Brazilian Journal of Chemical Engineering*, 10, 404-418.
- [29] Laoufi, N., Tassalit, D., Bentahar, F. (2008). The Degradation of Phenol in Water Solution by TiO_2 Photocatalysis in a Helical Reactor. *Global Nest Journal*, 10(3):404-418.
- [30] Xiao, X., Hao, R., Liang, M., Zuo., Xiaoxi, Nan, J., Li, L., Zhang, W. (2012). One-pot Solvothermal Synthesis of Three-Dimensional (3D) BiOI/BiOCl Composite with Enhanced Visible-Light Photocatalytic Activities for the Degradation of Bisphenol-A. *Journal of Hazardous Materials*, 233:122-130.
- [31] Anandan, S., Ohashi, N., Miyauchi, M. (2010). ZnO -based visible-light photocatalyst: Band-gap engineering and multi-electron reduction by co-catalyst. *Applied Catalysis B: Environmental* 100(3-4), 502-509.
- [32] Tsuzuki, T., McCormick, P. G. (2004) Mechanochemical synthesis of nanoparticles. *Journal of Material Science*, 39, 5143–5146.
- [33] Chen, S., Zhao, W., Liu, W., Zhang, S. J. (2009). Preparation, characterization and activity evaluation of p-n junction photocatalyst p-NiO/n-ZnO. *Journal of Sol-Gel Science and Technology*, 50:387–396.
- [34] Cho, M., Chung, H., Choi, W., Yoon, J. (2004). Linear correlation between inactivation of *E. coli* and OH radical concentration in ZnO photocatalytic disinfection. *Water Research*, 38, 1069–1077.
- [35] Yang, Z., Lv, L., Dai, Y., Xv, Z., Qian, D. (2010). Synthesis of ZnO-SnO_2 composite oxides by CTAB-assisted co-precipitation and photocatalytic properties. *Applied Surface Science* 256(9), 2898-2902.
- [36] Kumar, K., Chitkara, M., Sandhu, I.S., Mehta, D., Kumar, S. (2014). Photocatalytic, optical and magnetic properties of Fe-doped ZnO nanoparticles prepared by chemical route. *Journal of Alloys and Compounds* 588, 681-689.
- [37] Selvam, K., Muruganandham, M., Muthuvel, I., Swaminathan, M. (2016). The influence of inorganic oxidants and metal ions on semiconductor sensitized photodegradation of 4- fluorophenol. *Chemical Engineering Journal* 128(1), 51-57.
- [38] Sauer, T. P., Casaril, L., Oberziner, A. L. B, Jos´e, H J, Moreira, R. P. (2015) Advanced oxidation processes applied to tannery wastewater containing Direct Black 38 Elimination and degradation kinetics. *Journal of Hazardous Materials*, 135 274–279 doi:10.1016/j.jhazmat.2005.11.063.
- [39] Moore, D., Wang, Z.L. (2016). Growth of anisotropic one-dimensional ZnS nanostructures. *Journal of Materials Chemistry* 16(40), 3898-3905.